Frontiers in Bioscience Landmark

Front. Biosci. (Landmark Ed) **2023**; 28(6): 130
https://doi.org/10.31083/j.fbl2806130

Original Research

A Comprehensive Analysis of Prognostic Indicators in Serous Ovarian Cancer Based on Leukocyte Migration and Immune Microenvironment

Junping Pan[1,†], Xiaochuan Chen[1,†], Lin Yang[2,†], Yanwen Song[1], Jing Liu[2], Li Li[2], Yibin Lin[2], Lina Tang[3,*], Sufang Qiu[1,*], Qin Xu[2,*]

[1]Department of Radiation Oncology, Clinical Oncology School of Fujian Medical University, Fujian Cancer Hospital, 350011 Fuzhou, Fujian, China
[2]Department of Gynecology, Clinical Oncology School of Fujian Medical University, Fujian Cancer Hospital, 350011 Fuzhou, Fujian, China
[3]Department of Ultrasound, Clinical Oncology School of Fujian Medical University, Fujian Cancer Hospital, 350011 Fuzhou, Fujian, China
*Correspondence: 407062881@qq.com (Lina Tang); sufangqiu@fjmu.edu.cn (Sufang Qiu); 1379423879@qq.com (Qin Xu)
†These authors contributed equally.

Academic Editors: Juan Zhou and Pei-Fang Chen
Submitted: 27 November 2022 Revised: 27 January 2023 Accepted: 10 February 2023 Published: 30 June 2023

Abstract

Background: High-grade serous ovarian cancer (HGSOC) treatment is facing clinical challenges. The tumor immune microenvironment (TME) has recently been shown to perform a critical function in the prediction of clinical outcomes as well as the effectiveness of treatment. Leukocyte migration is enhanced in malignant tumors and promotes immunity. However, its role in how to underlie the migration of immune cells into the TME remains to be further explained in HGSOC. **Methods**: We built a prognostic multigene signature with leukocyte migration-related differentially expressed genes (LMDGs), which is associated with TME by single-sample gene set enrichment analysis (ssGSEA), in the The Cancer Genome Atlas (TCGA) cohort. Furthermore, we systematically correlated risk signature with immunological characteris-tics in TME, mutational profiles of HGSOC, and potential value in predicting efficacy of platinum-based chemotherapy and immunotherapy. Screening of the most important prognostic factor among risk signatures by Friends analysis, and immunofluorescence was employed to examine both the expression of CD2 as well as its relationship with CD8 and PD-1. **Results**: LMDGs-related prognostic model showed good prediction performance. Patients who had high-risk scores exhibited significantly reduced progression-free survival (PFS) and overall survival (OS) than those with low-risk scores, according to the results of the survival analysis ($p < 0.001$). In the TCGA cohort, the risk signature was found to have independent prognostic sig-nificance for HGSOC (HR =1.829, 95% CI = 1.460–2.290, $p < 0.001$) and validated in the Gene Expression Omnibus (GEO) cohort. Samples with high-risk scores had lower levels of CD8+ T cells infiltration. The low-risk signature shapes an inflamed TME in HGSOC. Furthermore, immune therapy might be effective for the low-risk subtype of HGSOC patients ($p < 0.001$). Friends analysis revealed that CD2 was the most important prognostic gene among risk signatures. Real-time quantitative PCR analysis showed the expression of CD2 was greater in tumor cells as opposed to normal ovarian cells. CD8, PD-1, and CD2 were shown to be co-localized in HGSOC tissues, according to immunofluorescence analyses. CD2 was significantly correlated with CD8 (r = 0.47). **Conclusions**: Our study identified and validated a promising LMDGs signature associated with inflamed TME, which might offer some prospective clinical implications for the treatment of SOC. CD2 might be a novel biomarker to predict immune efficacy.

Keywords: leukocyte migration; HGSOC; inflamed TME; CD2; TCGA

1. Introduction

Ovarian cancer (OC) has been shown to have the worst prognosis when compared to other gynecologic cancers. High-grade serous ovarian cancer (HGSOC), the most common kind of epithelial ovarian cancer (EOC), is usually diagnosed in an advanced stage [1,2]. HGSOC accounts for more than 80% of advanced-stage ovarian cancers and over 70% of all ovarian cancer deaths [3,4]. At present, the 5-year survival rate for HGSOC is roughly 47%, with the majority of these deaths occurring as a result of recurrence and chemoresistance [5]. In most cases, the surgery is accompanied by platinum-based chemotherapy as part of the standard therapy for HGSC. To overcome chemoresistance, a strong emphasis has been placed on targeted treatments, including anti-angiogenic and poly (ADP-ribose) polymerase (PARP) inhibitors, which have shown promising results when used for maintenance or recurrent disease treatment [6–10]. Nevertheless, long-term outcomes still pose significant challenges, with the prognosis for advanced stage patients remaining poor.

Numerous clinical studies for HGSOC are now focusing on immunotherapy. However, emerging clinical data have shown limited clinical efficacy of immunotherapy in ovarian cancer, with an objective response rate of 10–15%, which may be related to the highly immunosuppressive tumor microenvironment [11]. Zhang *et al.* [10] found that tumor-infiltrating T cells were significantly associated with median progression-free time (22.4 months vs 5.8 months, $p < 0.001$) and overall survival (50.3 months vs 18.0 months, $p < 0.001$) compared with tumors lacking T cells improved correlation, which provides strong evidence for the importance of the local tumor immune microenvi-

ronment in ovarian cancer. A commonly ignored factor affecting the efficacy of T cell-based immunotherapy is the capacity of effector T cells to migrate into and localized inside tumors, and also their ability to reach tumor antigens [12]. Leukocyte migration is of primary importance for an anti-tumor immune response, which occupies a pivotal function in the distribution of immune cells throughout the body [13]. Research has illustrated that leukocyte migration is enhanced in malignant tumors and promotes immunity [14]. As genome sequencing methods have improved, an increasing number of genomic signatures have been created to predict patient prognosis and treatment response. However, the significance of leukocyte migration-related genes in HGSOC and their relationship with tumor microenvironment (TME) remains unknown.

Therefore, our study aimed to systematically assess the association of leukocyte migration with HGSOC prognosis and TME. Then, using the single-sample gene set enrichment analysis (ssGSEA) approach in the TCGA cohort, we built a predictive multigene signature containing leukocyte migration-related differentially expressed genes (LMDGs) and verified it in the GEO cohort. Subsequently, we applied functional enrichment analysis to elucidate the fundamental processes of immune response mediation. Further analysis demonstrated that CD2 could be considered as a new biomarker in HGSOC.

2. Materials and Methods

2.1 Samples and Data Sets

The data were acquired from the TCGA database (https://portal.gdc.cancer.gov/) and comprised normalized whole-genome mRNA expression data of 379 HGSOC samples, somatic mutation data, and corresponding clinical data. After removing 1 patient without complete survival information, 378 HGSOC patients with simultaneously accessible OS and mRNA expression profile data were included in the study. GSE149940 and GSE32062 were extracted from GPL4133 and GPL6480 using the GEO database (http://www.ncbi.nlm.nih.gov/geo). The validation cohort (GSE32062) were external cohorts. The platform annotation files downloaded from the database were adopted to convert the probe data in the matrix files into gene symbols. To eliminate the batch effect, the "sva" R package (https://bioconductor.org/packages/release/bioc/html/sva.html) was utilized [15]. These data were obtained from publicly available web sources and we conducted this research in accordance with applicable protocols regarding the use of databases.

2.2 Cell Lines and Cell Culture Reagents

The human ovarian carcinoma SKOV3 cell lines and normal ovarian cell line IOSE80 were obtained from (ATCC, Manassas, VA, USA). IOSE80 cells were cultured in RPMI-1640 medium (BasalMedia, L210KJ, Shanghai, China) with 10% fetal bovine serum (Gibco, cat. no. 10270-106, Thermo Fisher Scientific, Waltham, MA, USA), and SKOV3 cells were cultured in McCoy's 5a Medium (cat. no. 30-2007, American Type Culture Collection (ATCC)) with 15% fetal bovine serum. Cells were cultivated at 37 °C in a humidified atmosphere containing with 5% CO_2. All cell lines were authenticated shortly before use by the short tandem repeat (STR) profile, carried out by Genewiz (Genewiz, Suzhou, China) and Genetic Testing Biotechnology Corporation (Genetic Testing Biotechnology Corporation, Suzhou, China). Cells were routinely tested for mycoplasma by PCR.

2.3 Identification of LMRGs Set

The immune cells marker gene sets were acquired from another publication [16]. Furthermore, for each immune-related cell, the R package "gsva" (https://bioconductor.org/packages/release/bioc/html/GSVA.html) was utilized to perform ssGSEA to calculate the enrichment score [17]. The "ConsensusClusterPlus" algorithm (50 iterations, resample rate of 80%) was used to cluster the HGSOC samples into three distinct groups (low-, medium-, and high-immunity) according to immune cell enrichment scores in ssGSEA [18]. To confirm that the three subgroups had distinct immunological profiles, we employed the R package "estimate" (https://bioinformatics.mdanderson.org/estimate/rpackage.html) to determine the immune, ESTIMATE, and stromal scores of each tumor sample [19]. Differential expression analysis of DEGs between low- and high-immunity groups was realized using the "limma" R package (https://bioconductor.org/packages/release/bioc/html/limma.html) [20]. $p < 0.05$ and $|\log2 \text{ fold change (FC)}| > 1.0$ were adjusted as thresholds. Additionally, The Molecular Signatures Database (MSigDB) (https://www.gsea-msigdb.org/gsea/msigdb/index.jsp) was used to retrieve leukocyte migration sets. Then, the Venn diagrams were plotted to detect leukocyte migration-related differentially genes (LMRGs) using the R package "VennDiagram" (http://cran.r-project.org/web/packages/VennDiagram/index.html) [21].

2.4 Development and Validation of a Prognostic Model Based on LMRGs

In order to generate a prognostic multigene signature in the training set, univariate Cox analysis and LASSO regression analysis were conducted. The "glmnet" R package (https://cran.r-project.org/web/packages/glmnet/index.html) was used to implement the abovementioned processes [22]. In order to calculate the risk score, the following equations were used: risk score = $\sum$ (expression level of each gene $\times$ corresponding regression coefficient). We categorized the patients into two groups according to the median value of risk score as the cutoff, namely: low-risk and high-risk groups. In addition, the Kaplan-Meier curve and the "survival" R package (https://cran.r-project.org/web/packages/survival/index.html) were used to ex-

amine variations in survival rates. Time-dependent ROC curves for 1-, 3-, and 5-year survival were plotted to appraise the prediction performance of the model. Furthermore, in the TCGA cohort, we utilized univariate and multivariate Cox regression analyses for OS to evaluate the prognostic association between the risk signature and other clinical parameters (such as age, stage, residual tumor, and TCGA subtype). Finally, using the GEO cohort (GSE32062) as external validation set, a similar approach was used to test the reliability and generality of the risk signature.

2.5 Gene Set Enrichment Analysis

GSEA was utilized to determine if a previously established gene set exhibited obvious differential expression between the low- and high-risk groups in the enrichment of MSigDB Database (c2.cp.kegg and c5.go.bp. v7.2. symbols.gmt). Then, it was assumed that the phenotypic labels were represented by the low- and high-risk and gene set permutations were undertaken 1000 times for each analysis. Classification of the gene ontology (GO) and Kyoto Encyclopedia of Genes and Genomes (KEGG) pathways that were enriched in differential phenotype was done using the normalized enrichment score (NES) and the false discovery rate (FDR).

2.6 Analysis of the Immunological Properties of TME

The TME in HGSOC exhibits immunological properties such as activation of the anticancer immunity cycle, tumor infiltrating immune cells (TIICs) infiltration, and expression of inhibitory immune checkpoints and immunomodulators. From the study conducted by Charoentong *et al*. [23], we initially compiled data on 92 immunomodulators, such as receptors, chemokines, and MHC. In the anticancer immune response, there are seven steps inside this cancer immunity cycle [24]. These steps and their influence on the ultimate fate of tumor cells were examined by Xu *et al*. [25] using ssGSEA, based on the gene expression levels of individual samples. Thereafter, in order to reduce the possibility of computation mistakes, we computed the infiltration levels of TIICs using seven separate algorithms: xCell, Cibersort-ABS, TIMER, quanTIseq, MCP-counter, Cibersort, and EPIC [25–30]. Using earlier research, we were able to identify the effector genes of TIICs.

Then, type I interferon (IFN) response and its marker genes were obtained from Akul's study [31]. From Auslander's investigation [32], we also obtained ten inhibitory immune checkpoints with treatment significance for further evaluation. The other gene sets, which present T cell-inflamed gene expression profile (GEP) or immune cytolytic activity (CYT), were collected from earlier studies [33,34]. Finally, we obtained the T cell receptor (TCR) and B cell receptor (BCR) Shannon Entropy data from Vésteinn Thorsson *et al*. [35].

2.7 Somatic Mutation Analysis

In order to identify single nucleotide variants (SNVs), single nucleotide polymorphisms (SNPs), and insertion-deletions (INDELs), we utilized the WES somatic mutations data from both the low-risk (n = 136) and high-risk (n = 135) groups with the aid of VarScan2.39 program. The Fisher's exact test was utilized to assess the differential mutation genes that had a p-value < 0.05. The somatic mutations were visualized utilizing the "maftools" R package (https://www.bioconductor.org/packages/release/bioc/html/maftools.html). Furthermore, aneuploidy scores and homologous recombination deficiency (HRD) score was obtained from Vésteinn Thorsson *et al*. and Taylor *et al*. [35,36]. Mutant-allele tumor heterogeneity (MATH) and Tumor mutation burden (TMB) was obtained from the somatic mutation data of 271 tumor samples, using "maftools" R package [37,38].

2.8 Prediction of the Response of Comprehensive Therapy

The Genomics of Drug Sensitivity in Cancer (GDSC) (https://www.cancerrxgene.org/) was used to estimate each patient's chemotherapeutic response. Ridge regression was employed to evaluate the half-maximal inhibitory concentration (IC50) and the "pRRophetic" R package (https://github.com/paulgeeleher/pRRophetic) was used to conduct 10-fold cross-validation [39].

We used two computational approaches to anticipate the immunotherapy response in HGSOC patients at low- and high-risk groups in order to investigate the association between the immunological signature and immunotherapy effectiveness. To begin with, Tumor Immune Dysfunction and Exclusion (TIDE) (http://tide.dfci.harvard.edu) was utilized to anticipate each sample's anti-CTLA4 and anti-PD1 immunotherapy response on the basis of the transcriptome patterns [40]. Second, we retrieved patient immunophenoscore (IPS) from The Cancer Immunome Atlas [23].

2.9 Real Time PCR and Immunofluorescence (IF) Staining Analysis

Real time PCR was performed as previously described [41]. The expression levels of CD2 were measured by normal ovarian cell (IOSE80) and ovarian cancer cell (SKOV3) on ABI 7700 system using the following primers: forward CD2-F: 5′-TCAAGAGAGGGTCTCAAAACCA-3′, reverse CD2-R 5′-CCATTCATTACCTCACAGGTCAG-3′; GAPDH-F: 5′-TGACTTCAACAGCGACACCCA-3′, reverse GAPDH-R 5′-CACCCTGTTGCTGTAGCCAAA-3′. Total RNA from cultured cells was isolated at 80% confluence with TRIzol reagent (T9424, Sigma Aldrich, STL, USA). Total RNA (1 µg) was reverse transcribed into cDNA using a reverse transcription kit (Takara, Japan). Real-time PCR was performed using SYBR Premix Ex Taq (Takara, Otsu, Japan) according to the manufacturer's instructions.

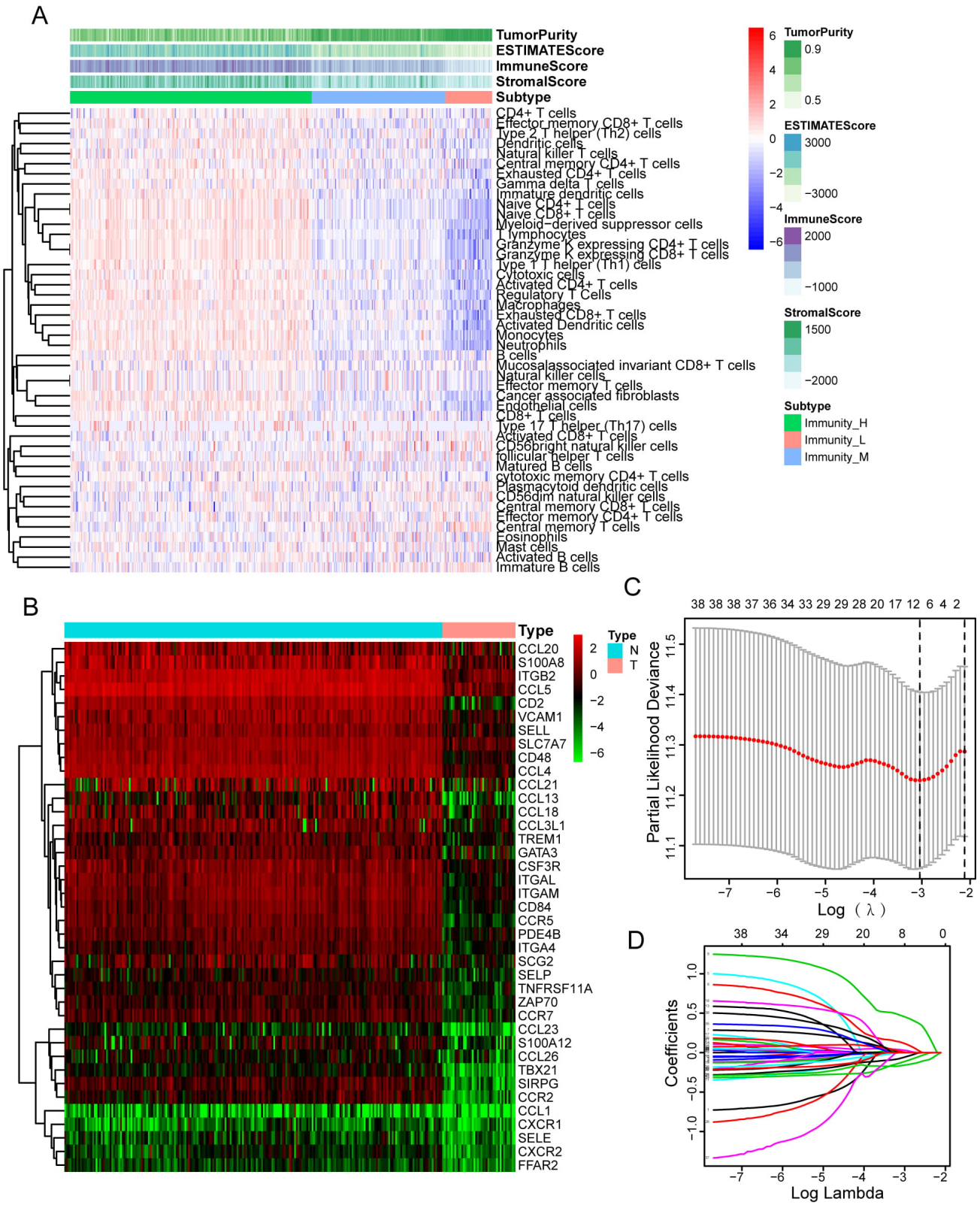

Fig. 1. Immune microenvironment clustering of HGSOC and Construction of Prognosis Prediction Model. (A) There are 48 immune-related gene sets in ssGSEA that have been enriched in HGSOC cancer The gene sets are comprised of immune processes and immune cells. This heatmap also displays the tumor purity, stromal scores, immune scores, and ESTIMATE scores. (B) Comparison of leukocyte migration-related differential expression genes (DEGs) of low- and high-immune infiltration groups in this heatmap. (C) Nine genes were found to be correlated with the prognosis according to the LASSO Cox analysis. (D) 1000-round cross-validation. was used to determine the best values for the penalty parameter.

PCR reaction conditions: denaturation at 95 °C for 10 s, annealing at 60 °C for 15 s, and extension at 72 °C for 30 s. This cycle is amplified for 45 times, and the melting curve is analyzed after the cycle. 23 HGSOC samples (OC-1601) were procured from Servicebio Company (Wuhan, China) and utilized to IF with anti-human CD2 (ab4055, Abcam, MA, USA), anti-PD-1 antibody (ab213524, Abcam, MA, USA) and CD8-specific antibody (ab4055, Abcam, MA, USA). We evaluated only the proportion of cells that had a high membrane staining intensity (brown staining) for CD2 and CD8. The corresponding secondary antibodies included CY5-TSA (G1224, Servicebio), which was utilized to detect PD1, FITC-TSA (G1223, Servicebio), which was utilized to detect CD8, and CY3-TSA (G1222, Servicebio), which was utilized to detect CD2. DAPI was used to highlight the nuclei. Lastly, we calculated the percentages of positive cells across the field.

2.10 Single-Cell Level Analysis

In order to categorize tumor, stromal, and immune cells, we implemented hierarchical clustering based on the ovarian Cancer (OV) single-cell sequencing data (GSE118828) collected from the electronic website of the Tumor Immune Single-cell Hub (TISCH) (http://tisch.comp-genomics.org/) [42,43]. After that, the expression of CD2 in these cells was determined, and the findings were shown graphically using scatter plot.

2.11 Statistical Analysis

R software version 4.0.3 (https://www.r-project.org/) was utilized to conduct all statistical analyses and plot drawings. The unpaired Student's *t*-test and the Whitney U-test were utilized to compare variations between two groups with normal distributed and non-normal distributed variables, respectively [44]. Categorical variables were compared utilizing a Chi-square test [45]. With regard to non-parametric data, the Wilcoxon rank-sum test was employed when two groups were involved, whereas the Kruskal-Wallis test was employed when more than two groups were involved. Using Pearson's chi-square test, correlations between qualitative variables were examined. A *p*-value less than 0.05 was interpreted as having statistical significance if it was not indicated above.

3. Results

3.1 Immune Microenvironment Landscape of HGSOC and Construction of Prognosis Prediction Model

With the application of the ssGSEA method, 48 infiltrating immune cells were integrated into HGSOC tissues in order to measure their immunological capability (Fig. 1A). Consensus clustering analysis was used to categorize the overall TCGA cohort into three different groups (high-immunity: 217 samples; median-immunity: 120 samples, and low-immunity: 42 samples). For the purpose of validating the immunity of the three immune groups, we included the ESTIMATE, the immune, and the stromal scores in the heatmap (Fig. 1B). We discovered that when compared to the group with low immunity, the group with high immunity exhibited stronger immune components as well as lesser tumor purity.

To examine the function of leukocyte migration in modulating microenvironment immunity of HGSOC, we performed limma analysis to identify 39 differentially expressed leukocyte migration-related genes in the low- and high-immunity group (Fig. 1B, **Supplementary Table 1**). Then, Univariate Cox and LASSO regression analyses were carried out in order to detect significant prognostic biomarkers, and the results were used to create a risk signature (Fig. 1C,D). The formula for the risk signature was determined using corresponding coefficients: risk score = 0.6054 × CXCR2 - 0.2539 × CCR7 - 0.2659 × SELL - 0.0251 × CD2 + 0.0127 × TREM1 - 0.8400 × TBX21-0.1818 × CCL13 + 0.3648 × ITGAM + 0.4273 × SIRPG.

3.2 Clinical Prognostic Significance of Risk Signature in the TCGA and GEO Databases

HGSOC samples were categorized into low- and high-risk groups according to their median risk score. The Kaplan-Meier curve revealed that the high-risk group samples exhibited poorer overall survival (OS) and progression-free survival (PFS) as opposed to the low-risk group samples, demonstrating that the prognostic signature of the risk score is efficacious for predicting survival. Notably, the data from the GEO (GSE32062) database was used to validate this finding (Fig. 2A,B). In addition, by applying receiver operating characteristic curve analysis on the TCGA data, it was discovered that risk signature was a strong predictor for 1-year (AUC = 0.646), three-year (AUC = 0.634), and five-year survivals (AUC = 0.685). The validity of this discovery was greatly increased by incorporating data gathered from the GEO database (AUC = 0.640, 0.595, 0.628) (Fig. 2C). Univariate Cox analysis revealed that risk signature (HR = 1.783; 95% CI = 1.440–2.207; $p < 0.001$), and tumor residual disease were both greatly associated with a dismal OS. The results of the Multivariate Cox analysis illustrated that high-risk signature in TCGA database (HR = 1.829; 95% CI = 1.420–2.290; $p < 0.001$) and in GEO database (HR = 1.287; 95% CI = 1.099–1.506; $p = 0.002$) exhibited an independent correlation with a worse OS (Fig. 3A,B). Consequently, our risk signature has the potential to serve as an independent prognostic marker for HGSOC, as shown by this finding.

Then, we explored relationships between risk signature and stage in HGSOC. According to the data from the TCGA and GEO databases, HGSOC patients showed significantly higher risk scores with the high stage as opposed to the low stage group patients (Fig. 3C). Interestingly, we discovered that the immunoreactive group had a lower risk score compared to patients in the other TCGA subgroups (Fig. 3D). These findings identify that risk signature is cru-

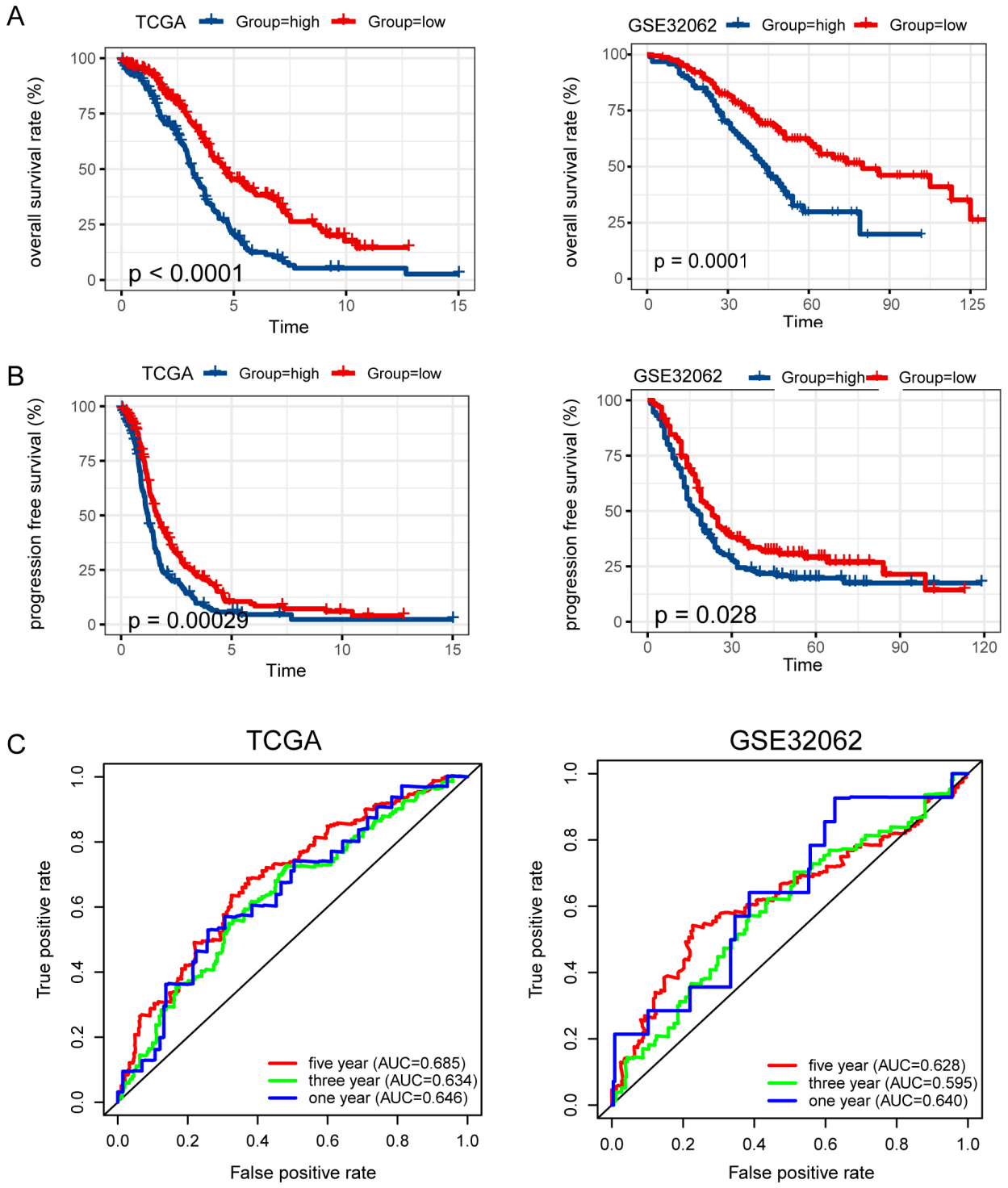

Fig. 2. The prognostic value of risk signature. (A) In the GEO and TCGA datasets, low-risk group patients had a favorable OS rate as opposed to those in the high-risk group. (B) In the TCGA and GEO datasets, low-risk group patients had a longer PFS as opposed to the high-risk group patients. (C) The ROC curve for 1-, 3-, and 5-year OS of HGSOC patients in the GEO and TCGA datasets.

cial to anti-tumor immunity.

3.3 Gene Set Enrichment Analysis

Gene set enrichment analysis was performed on the GO and KEGG databases utilizing the MSigDB database (FDR <0.05). NES was conducted to determine the GO and signaling pathways that were strongly enriched. In this research, antigen processing, as well as peptide antigen presentation through immune response regulating signaling pathway, MHC class I, positive modulation of T cell receptor signaling pathway, response to type I interferon, positive modulation of lymphocyte chemotaxis, antigen pro-

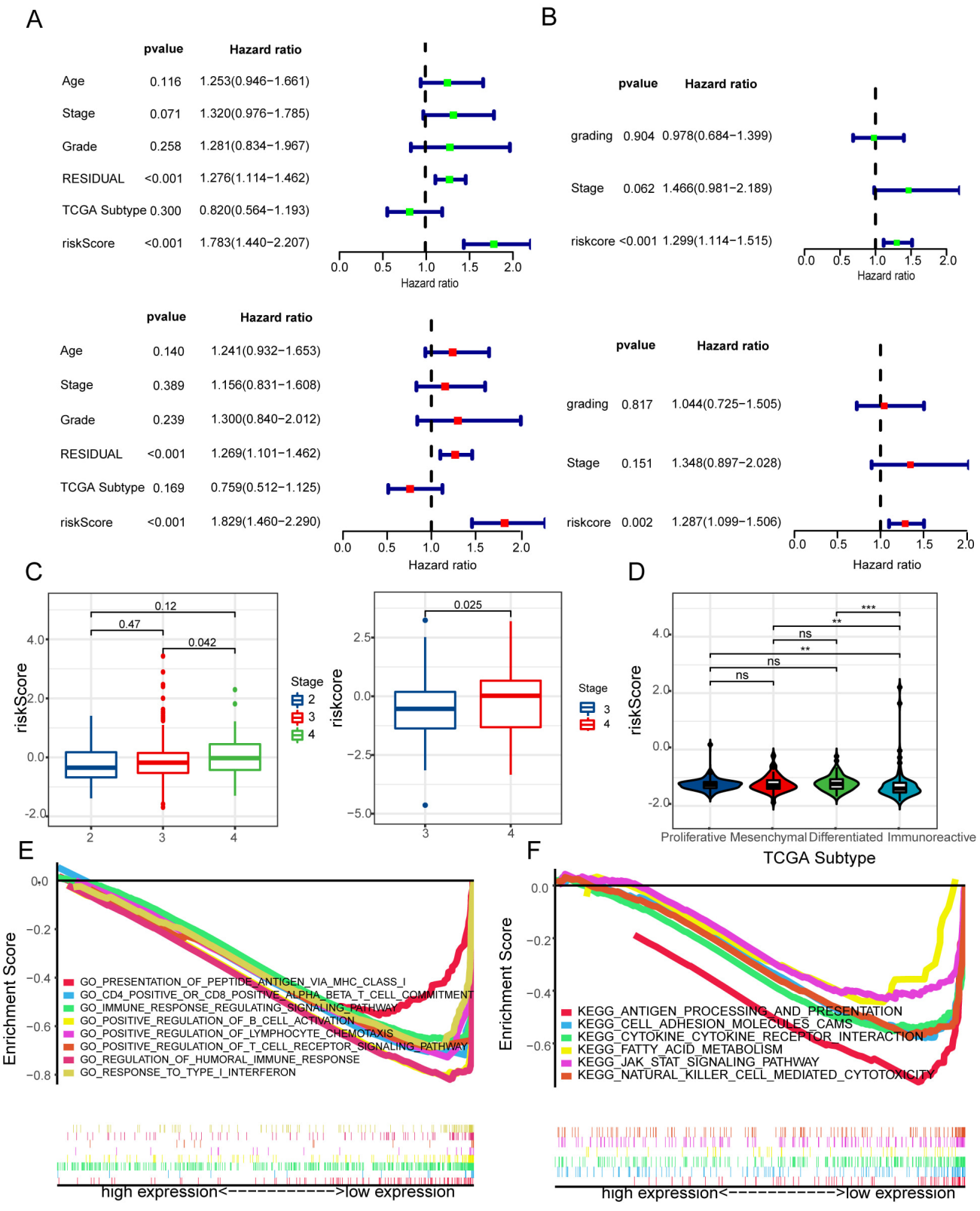

Fig. 3. Evaluation of the independent prognostic significance and GSEA enrichment analysis of risk signature. (A,B) Cox analyses, both univariate and multivariate, were used to determine the independent prognostic significance of the risk signature with regard to OS in glioma patients based on the CGGA and TCGA datasets. (C) Relationships between risk signature and stage in HGSOC. (D) Relationships between risk signature and TCGA subgroup in HGSOC. (E,F) GO and KEGG were evaluated utilizing the GSEA. $^{**}p < 0.01$, $^{***}p < 0.001$, $^{ns}p > 0.05$.

cessing and presentation, JAK_STAT signaling pathway, and cell adhesion molecules (CAMs), were enriched in low-risk phenotype (Fig. 3E,F).

3.4 The Low-Risk Signature Shapes an Inflamed TME in HGSOC

Depending on the proportion of cytotoxic immune cells infiltrating TME, the tumor can be described as either immunologically active 'inflamed' or immunologically passive 'non-inflamed' [46]. Risk signature was observed to exhibit a negative correlation with a vast proportion of immunomodulators (Fig. 4A). Most of the MHC molecules were downmodulated in the high-risk group, indicating that the ability to present and process antigens had been reduced. Three key chemokines (CXCR3, CXCL10, and CXCL9), which are required to recruit CD8+ T cells into the TME in HGSOC, were shown to be upmodulated in the low-risk group. Further investigation revealed that paired receptors and other chemokines such as CXCL13, CXCL11, CCL5, XCL2, and CCL4, exhibited a negative association with risk signature. These receptors and chemokines stimulate the mobilization of effector TIICs, including antigen-presenting cells and CD8+ T cells.

The cancer immunity cycle is a representation of our body's immunological response to cancer. The functions of the cancer-immunity cycle meticulously represent the ultimate impact of the intricate immunomodulatory interplay in the TME [24,25]. Most of the cycle steps were shown to be increased in the low-risk group, such as the production of cancer cell antigens (Step 1), priming and activation (Step 3), as well as immune cells transportation to tumors (Step 4) (recruitment of DC, NK cells, Macrophages, Th1 cells, and CD8 T cell) (Fig. 4B). Consequently, the decreased activity of these steps might result in a decrease in the infiltration levels of effector TIICs in the TME. Notably, the low-risk group had a decreased T cell activity in recognizing cancer cells (Step 6). The reason for this phenomenon might lie in the fact that the low-risk group had an elevated level of PD-L1 expression. Step 7 activity (cancerous cell death) was discovered to be upmodulated in the low-risk group.

Following that, we estimated the infiltration levels of TIICs utilizing seven separate algorithms provided by the TIMER website. In our result, risk signature was inversely associated with DC cells, B cells, and CD8+ T cells in the TCGA datasets (Fig. 4C). These results were confirmed in the Geo cohort (**Supplementary Fig. 1**). Similarly, risk signature was inversely associated with the CD8+ T cells effector genes, which was elevated in the low-risk group (Fig. 4D,E). Moreover, the marker genes of type I IFN response were a high expression in the low-risk group. The risk model was inversely associated with type I IFN response (Fig. 5A,B). Consistently, risk signature was observed to be inversely associated with most of the immune checkpoint inhibitors such as TIGIT, IDO1, TIM-3, LAG-3, PD-1, CTLA-4, and PD-L1 (Fig. 5C,D). Collectively, the low-risk signature shapes an inflamed TME.

Meanwhile, we discovered the risk signature strongly correlated with CYT and GEP in HGSOC, which both decreased in the low-risk group (Fig. 5E). Furtherly, we evaluated TCR and BCR repertoires from the TCGA HGSOC cohort. Mean TCR and BCR diversity values, which were measured by Shannon entropy, differed by the risk signature, with the highest diversity in the low-risk score groups (Fig. 5F). A powerful anti-tumor response may be associated with antigen-specific BCR and TCR repertoires that are essential for the identification of malignant cells and pathogens. Our finding indicated risk signature was strongly associated with the inflamed TME and anti-tumor response.

3.5 Mapping of Mutations Found in HGSOC

To find the relevant genetic alterations, we dissected the somatic mutations between the low and high-risk cohorts. The top 30 most commonly mutated genes in the corresponding cohorts are depicted in Fig. 6A. Then we explored the association between risk signature and measures of DNA damage, including aneuploidy score, homologous recombination deficiency (HRD). The low-risk group correlated negatively with aneuploidy score, positively with HRD (Fig. 6B,C). Due to lower leukocyte infiltration in high aneuploidy samples, aneuploidy was negatively associated with immunological signaling gene expression [36]. These results suggest that the risk signature of the affected immune infiltrations may be associated with aneuploidy. It has been hypothesized that the genetic instability exhibited in HRD tumors alters immunogenicity, making these malignancies highly sensitive to immunotherapy. We next calculated the TMB and MATH by the maftools R package. Despite the fact that the TMB was greater in the low-risk group as opposed to that of the high-risk group, this difference was not significant. No differences in MATH were found between the low- and high-risk groups (Fig. 6D). This result demonstrated that risk signature may serve as an immune marker independent of TMB and MATH.

3.6 Risk Signature Predicts the Response of Conventional Therapy

The commonly used treatment options for ovarian cancer include chemotherapy, targeted therapy, and immunotherapy. Platinum-based chemotherapy is the cornerstone of treating HGSOC. To determine the effect of Risk signature on Platinum-Based Chemoresistance in HGSOC, according to platinum-based response (whether to platinum resistance) and risk score, we categorized the samples in TCGA and GEO databases into four groups, including high-risk score groups with or without platinum resistance and low-risk score groups with or without platinum resistance. We found that no matter whether the risk score in HGSOC patients was high or low, patients who were sensitive about platinum had a longer survival time as opposed

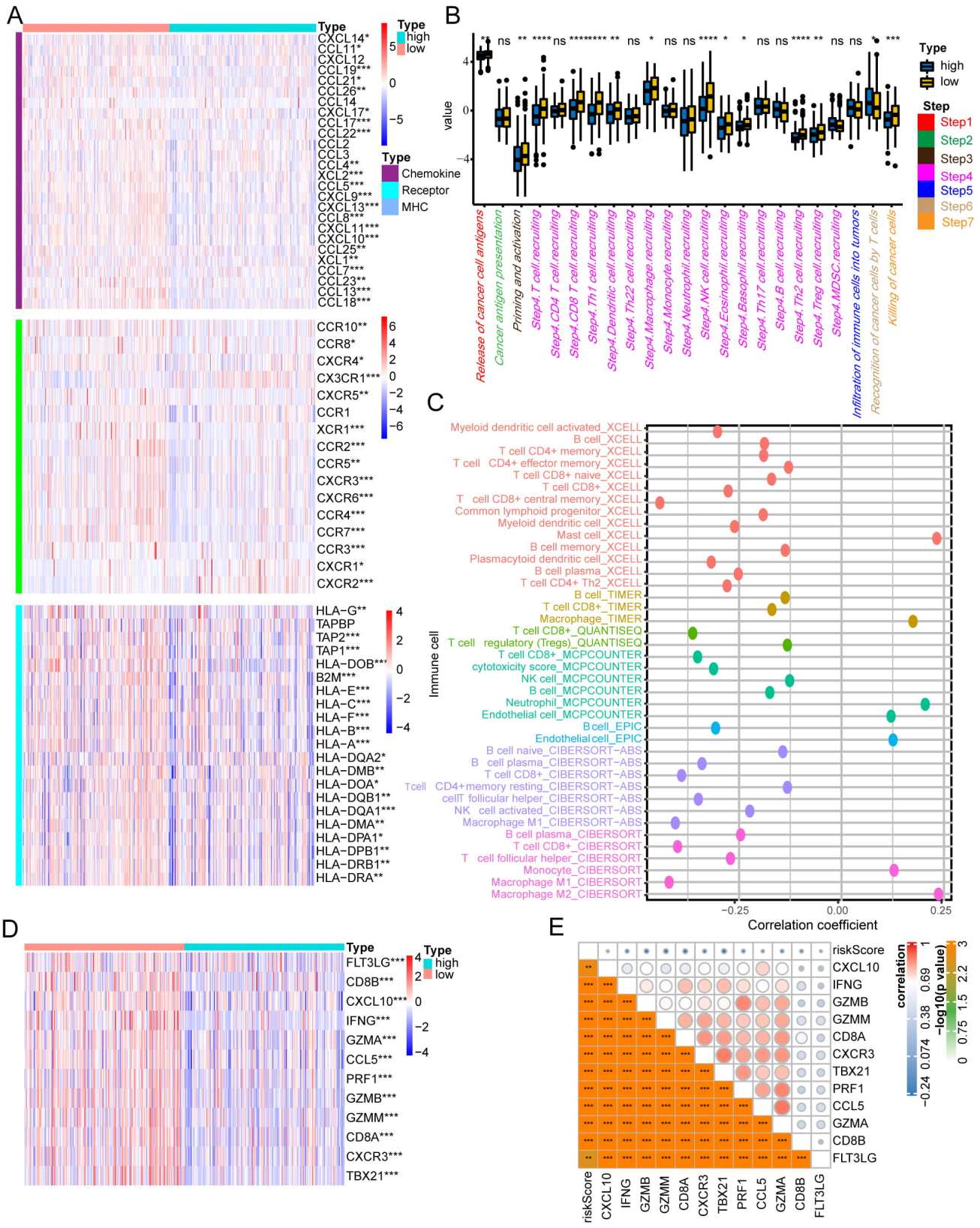

Fig. 4. The low-risk signature shapes an inflamed TME in HGSOC. (A) In HGSOC, there are differences in the expression of 122 immunomodulators (MHC, receptors, and chemokines). (B) Difference between low- and high-risk groups at distinct stages of the cancer immunity cycle. (C) Relationship between the risk score and infiltration levels of severe TIICs, as determined by seven separate algorithms. (D) Differences in the effector genes of CD8+ cells between low- and high-risk groups. (E) Relationship between risk score and CD8+ cell effector genes. *$p < 0.05$, **$p < 0.01$, ***$p < 0.001$, ****$p < 0.0001$, $^{ns}p > 0.05$.

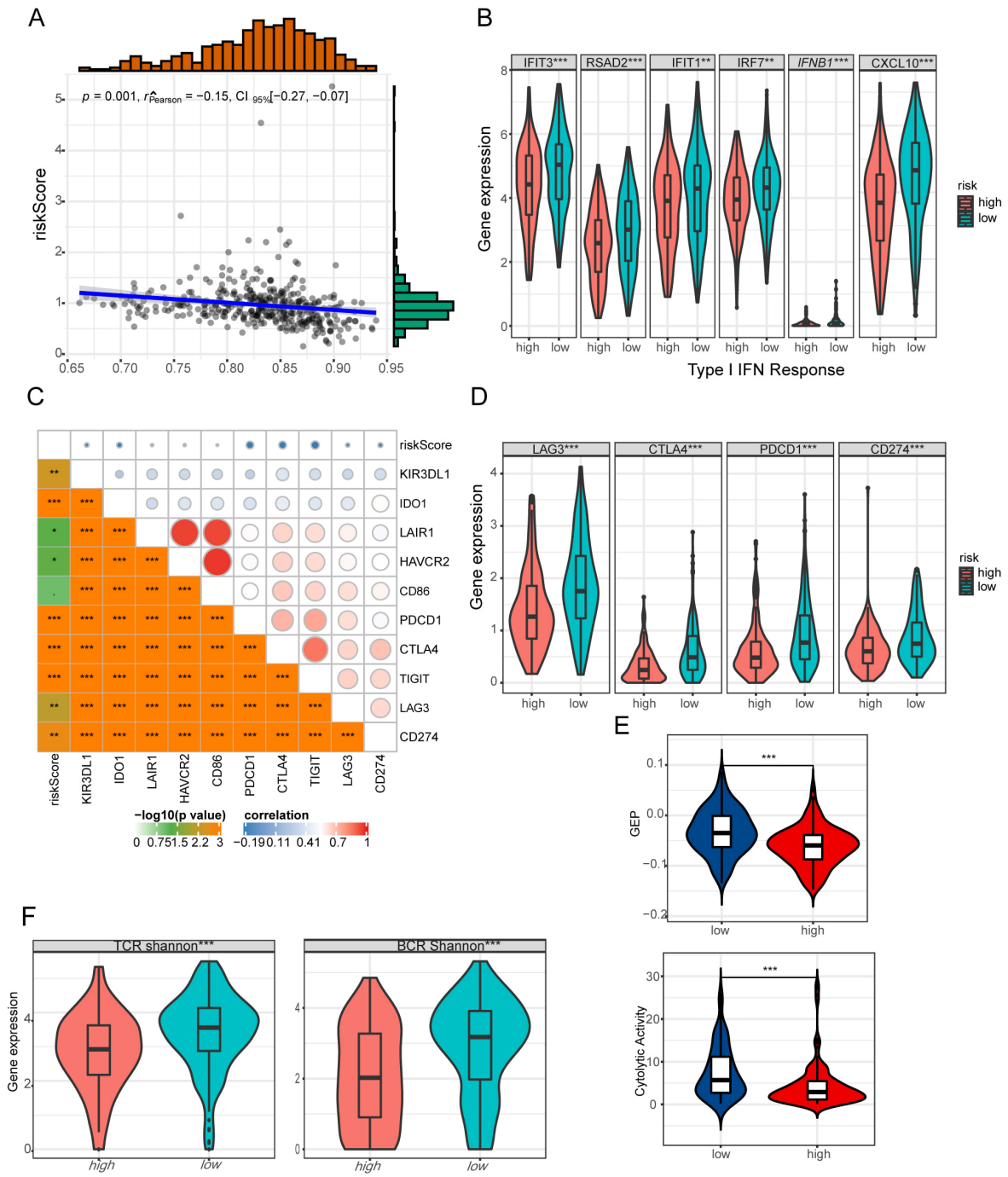

Fig. 5. The immune profile of risk signature in HGSOC. (A) Relationship between risk score and type I IFN response. (B) Differences in the effector genes of type I IFN signature between low- and high-risk groups. (C) Relationship between risk score and 10 inhibitory immune checkpoints. (D) Differences in PD1, PDL-1, CTLA4, LAG3 between low- and high-risk groups. (E) Differences in GEP and CYT between low- and high-risk groups. (F) Differences in TCR and BCR diversity values between low- and high-risk groups. $^{**}p < 0.01$, $^{***}p < 0.001$.

to those with platinum resistance. But the low-risk score group was found to have a survival advantage as opposed to the high group in HGSOC patients who were sensitive about platinum, but not those with platinum resistance (Fig. 7A). Moreover, patients with platinum resistance had a higher risk score (Fig. 7B). Furthermore, we estimated the IC50 for each subtype using the prediction model for the three agents developed by Xiaofan Lu [47]. The findings indicated that the low-risk group responded more favorably to chemotherapy as opposed to the high-risk group (cisplatin, $p < 0.01$; paclitaxel, $p < 0.001$; etoposide, $p < 0.001$) (Fig. 7C). Olaparib and Niraparib, the poly(ADP-ribose)

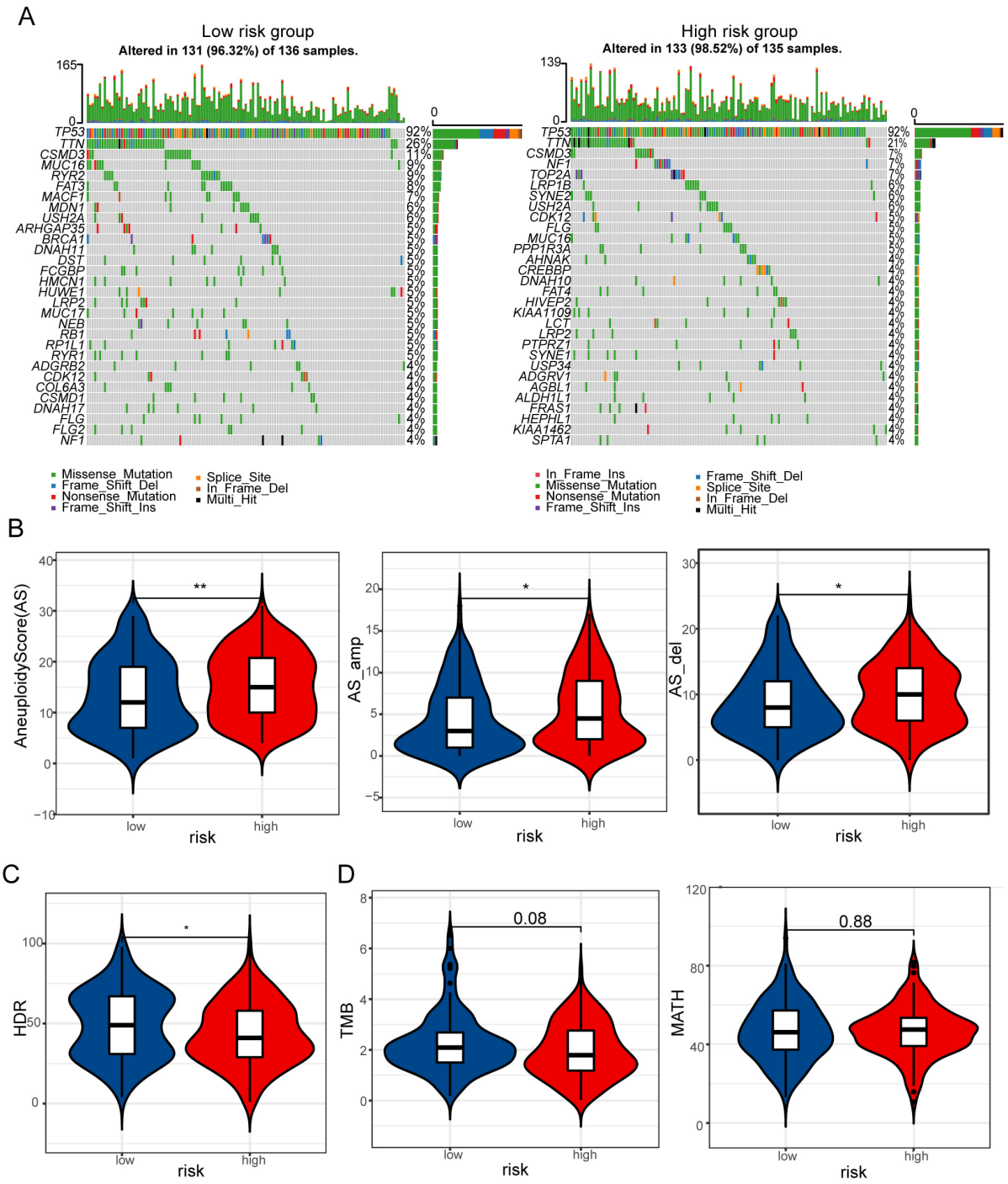

Fig. 6. Mapping of mutations found in HGSOC. (A) The top 30 commonly mutated genes between low- and high-METTL7B groups. (B) Differences in AS, including AS_amp and AS_del between low- and high-risk groups. (C) Differences in HDR between low- and high-risk groups. (D) Differences in TMB and MATH between low- and high-risk groups. *$p < 0.05$, **$p < 0.01$.

polymerase (PARP) inhibitors, were authorized for maintenance treatment of advanced HGSOC after first-line platinum chemotherapy [48]. We then analyzed the effect of risk signature on *PARP* inhibitors using the GEO database (GSE149960) (Fig. 7D). Results demonstrated that PARP inhibitor-resistance group tended to have higher risk scores than PARP inhibitor-sensitive group ($p = 0.03$). The findings above revealed that the risk signature can be used to identify potential groups of patients who gain benefit from PARP inhibitors and platinum-based chemotherapy.

Despite recent advances in the maintenance treatment of HGSOC, patients with locally progressive or metastatic HGSOC have been less successful in achieving satisfactory clinical results. We utilized the TIDE algorithm to estimate immune checkpoint blockade (ICB) treatment response in order to determine possible groups of patients

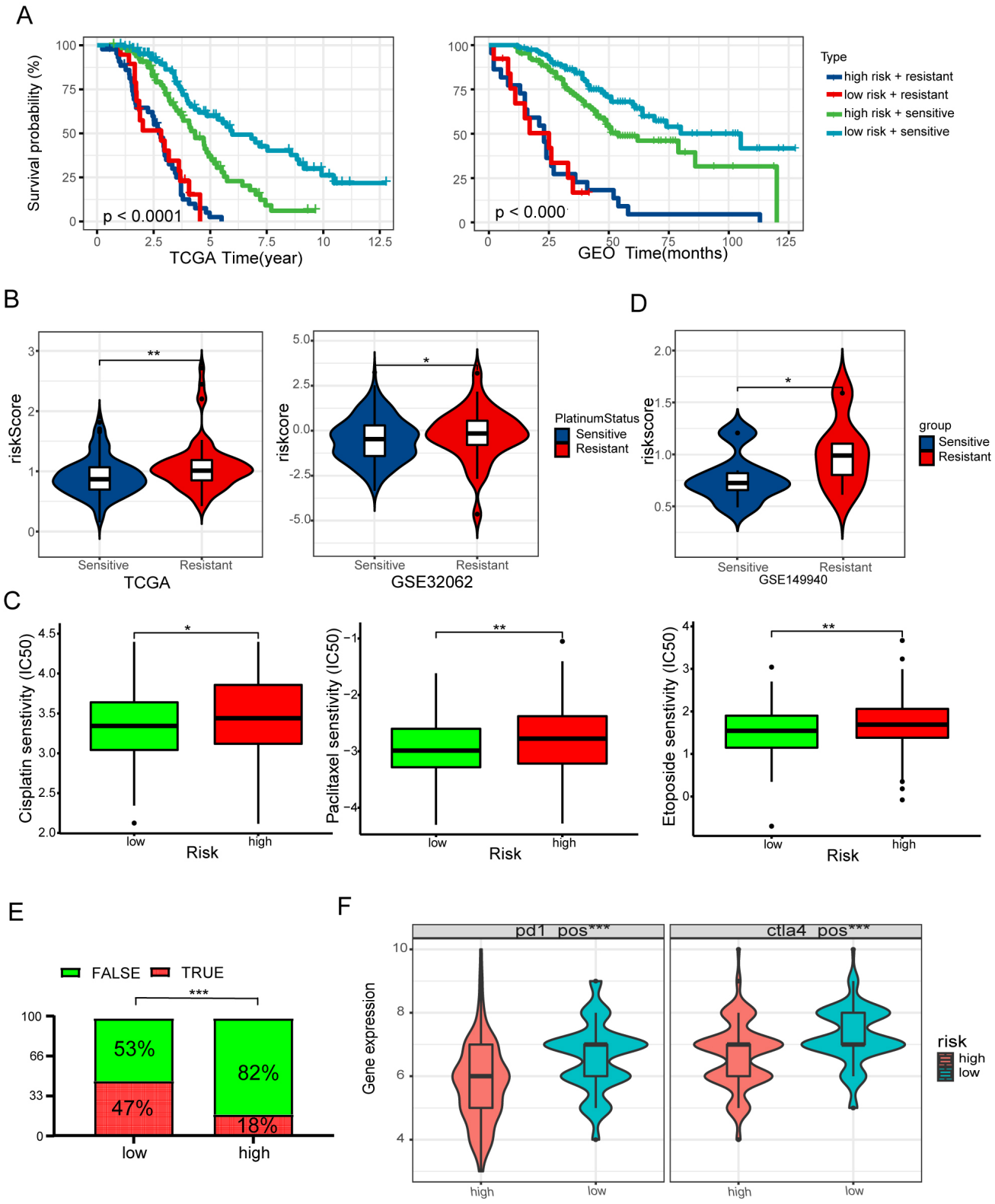

Fig. 7. Risk signature predicts the response of conventional therapy. (A) Kaplan-Meier curves of OS for the high-risk score with or without platinum resistance and low-risk score with or without platinum resistance in the TCGA and GEO cohort. (B) Differences in risk score between platinum resistance and platinum-sensitive groups. (C) Differences in risk score between PARP inhibitors resistance and PARP inhibitors sensitive groups. (D) The boxplots depict the estimated IC50 values for doxorubicin, paclitaxel, and cisplatin for three subtypes, as determined by the GDSC database. (E) The anticipated immunotherapy (TRUE/FALSE) response rate to anti-PD-L1 in low- and high-risk groups in the TCGA cohort. (F) Differences in IPS between low- and high-risk groups. *$p < 0.05$, **$p < 0.01$, ***$p < 0.001$.

who may gain benefit from immunotherapy. Results illustrated that the low-risk group displayed a significantly improved response to immunotherapy as opposed to the high-risk group (Fig. 7E). The Cancer Immunome Atlas (https://tcia.at/) showed similar results. The low-risk group exhibited a greater response rate to CTLA4 and PD-1 inhibitors, implying that patients who have low-risk scores may gain benefit from immunotherapy (Fig. 7F).

3.7 CD2 Expression, Survival, and Immune Infiltration Analyses

We further performed a Friends analysis of 9 risk genes by using GOSemSim R package to screen a hub gene, CD2 (Fig. 8A) [49]. Notably, the expression of CD2 was greatly decreased in normal tissues compared to HGSOC tissues using Gene Expression Profiling Interactive Analysis (GEPIA) (Fig. 8B,C) [50]. Based on the cellular level, the expression of CD2 was shown to be greater in tumor cell as opposed to normal ovarian cell by PCR (Fig. 8D). In the TCGA database, patients with HGSOC who exhibited low expression of CD2 had obviously poorer OS compared with those who exhibited high CD2 expression (Fig. 8E). Following that, the survival analysis was tested utilizing the GEO database (Fig. 8F).

TIICs of HGSOC samples were utilized to further explore the interaction between CD2 expression and the TME. Seven separate algorithms from the TIMER online platform were employed to analyze these TIICs. Results showed CD8+ T cells, dendritic cells, M1 macrophages strongly correlated with CD2, which offers convincing evidence for the critical function played by CD2 in the TME of HGSOC samples (**Supplementary Fig. 2**). Interestingly, the radar plot demonstrated that CD2 strongly correlated with immune checkpoint inhibitors (PD1, PDL1, CALT4, IDO1), TCR scores, BCR scores, GEP, and CYT, negatively correlated with TIDE score (Fig. 9A). Moreover, the group displaying elevated CD2 expression was found to have a considerably improved response to immunotherapy as opposed to the low group using the TIDE algorithm (Fig. 9B). Furthermore, multicolor immunofluorescence analysis demonstrated that CD2, PD-1, and CD8 were co-localized in HGSOC tissues, suggesting that CD2 and CD8+ cells spatially interact in the TME and optimizing the CD2 intensity in HGSOC tissue could enhance the effectiveness of immunotherapy by enhancing the anti-tumor immune responses (Fig. 9C,D). In addition, we found that the expression level of CD2 was higher in T cells compared with malignant cells and stromal cells in the OV patients (GSE118828) by using TISCH database (Fig. 9E).

4. Discussion

In the present research, we utilized RNA-seq data retrieved from TCGA together with 39 differentially expressed leukocyte migration-related genes to construct a prognosis-related 9-LMGs signature that can be used to establish risk classification and anticipate clinical outcomes in cancer patients. We discovered that there is a strong correlation between the risk signature and clinical-pathological factors. The efficiency of the risk signature as an independent prognostic indicator was validated using Cox regression. Immune-related pathways were shown to be significantly enriched in the low-risk group, as demonstrated by the functional enrichment analysis. We discovered that the risk signature was associated with the processes of the cancer immunity cycle. Furthermore, the high-risk group was inversely associated with a large number of immunomodulators and exhibited a suppressive immune microenvironment. Moreover, we examined the prognostic significance of risk score for HGSOC responses to different treatments. We discovered that patients in the low-risk group had a higher likelihood of benefiting from chemotherapy treatment as opposed to those in the high-risk group. ICB therapy might be efficacious for HGSOC patients with low-risk scores. Subsequent analysis demonstrated that CD2 was a hub gene related to TME, played a significant prognostic role in HGSOC patients. Tumors with elevated levels of CD2+ cell infiltration were shown to have a higher abundance of intratumoral PD1+ cells and CD8+ T cells infiltration, according to immunofluorescence analyses.

Leukocytes are immune cells that comprise both adaptive immune cells (T and B lymphocytes) and innate immune cells (NK cells, dendritic cells, macrophages, monocytes, granulocytes, etc.) [51]. The migration of leukocytes is critical for immune system development as well as in the response to tumor rejection, inflammation, and infection [52]. Several research reports have demonstrated that defects in the migration of NK cells to tumor locations resulted in the development of immune-suppressive TME [53]. Trafficking of T cells into the TME is key to the success of cancer immunotherapy, such as the adoptive cell transfer therapy [54]. Nevertheless, most studies mainly focused on chemokines, the proteins that modulate the migration of leukocytes, inducing the recruitment of protumorigenic immune cells while inhibiting the buildup of anti-tumorigenic immune cells. CXCR2 inhibition reduced the count of MDSC cells in tumors while increasing the number of T cells and natural killer cells [55]. In a previous study, CXCR3 was identified as a prognostic marker as well as a possible therapeutic target for individuals with solid malignancies [56]. Our findings revealed that risk classification based on integrated LMRG sets had a crucial function in the TME and prognosis of HGSOC patients

TME may be classified into two groups: those with T-cell inflammation (with positive CD8+ T-cell infiltration and also type I interferon features) and those without T-cell inflammation (lacking both). The TME with T cell–inflammation is often correlated with improved prognosis and enhanced susceptibility to ICB [57–59]. Here, we noted that the infiltration levels of CD8+ T cells were obviously elevated in the low-risk group, which enriched in the re-

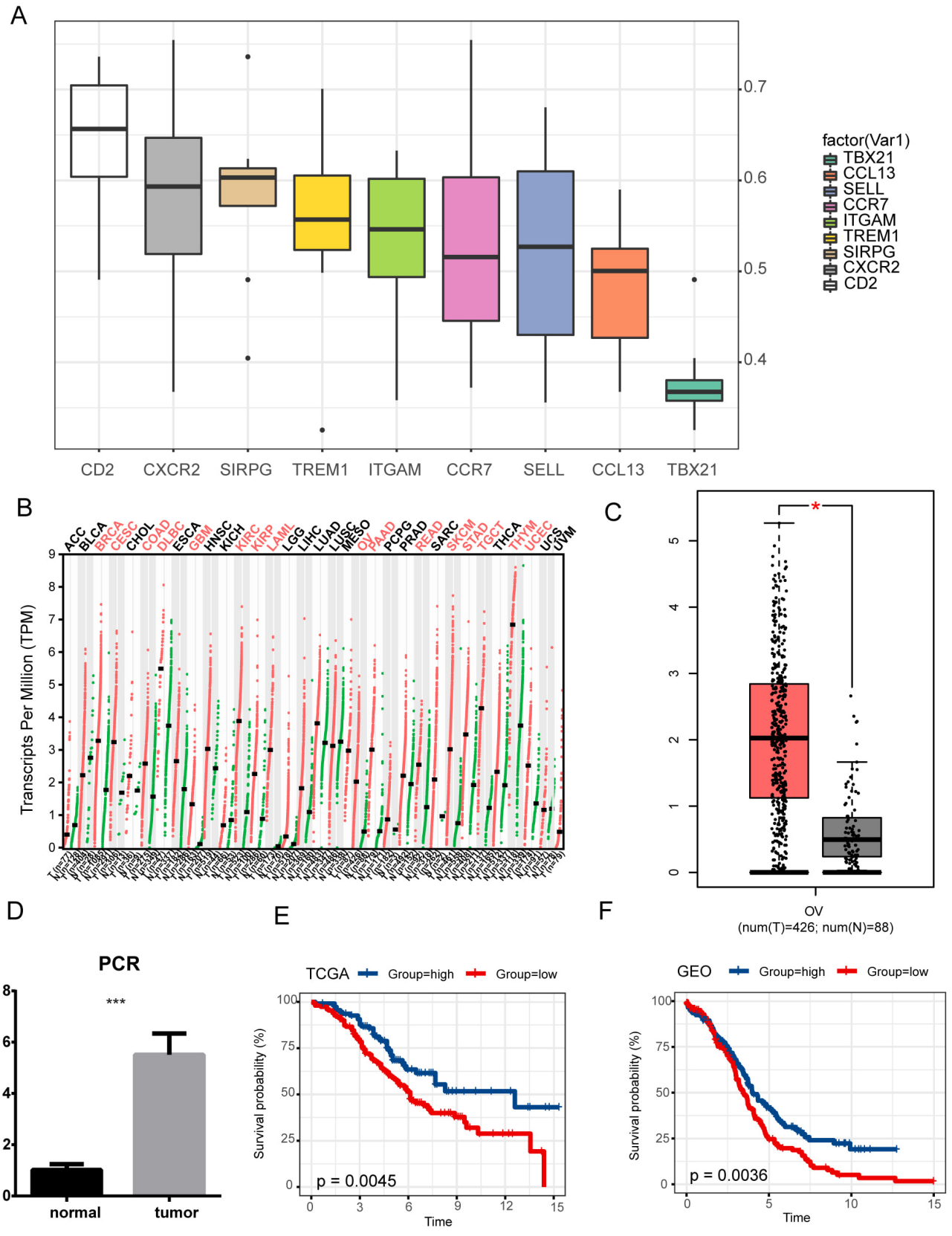

Fig. 8. CD2 Expression and Survival Analyses. (A) The boxplots of the estimated factor value for 9 LMDGs based on Friends analysis. (B) Pan-cancer analysis of CD2 expression across the cancerous tissue and the corresponding adjacent normal tissue from TCGA. (C) Differential expression of CD2 in HGSOC. (D) Real-time quantitative PCR analysis of CD2 expression in normal ovarian cells and skov3 ovarian cancer cells. (E,F) Kaplan-Meier curves of OS for CD2 in the GEO and TCGA cohorts. *$p < 0.05$, ***$p < 0.001$.

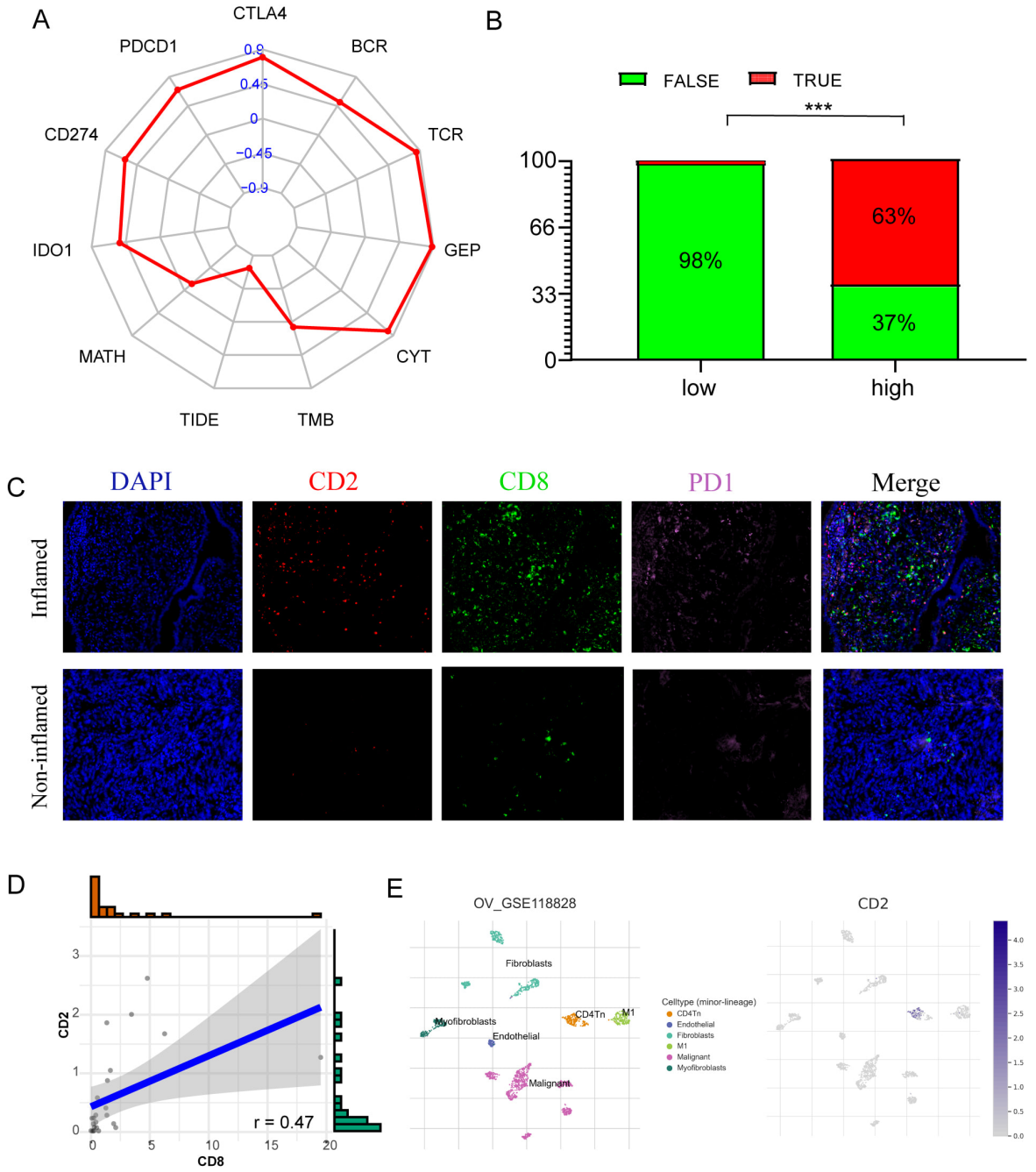

Fig. 9. Correlations between CD2, the immune infiltration, and the response of immunotherapy in HGSOC. (A) Radar graph of the correlation between CD2 and immune checkpoint inhibitors (PD1, PDL1, CALT4, IDO1), TCR scores, BCR scores, GEP, CYT, and TIDE score. (B) The anticipated immunotherapy (TRUE/FALSE) response rate to anti-PD-L1 in low- and high-risk CD2 in the TCGA cohort. (C) Expression of CD2, CD8, and PD-L1 in our cohort was detected using immunofluorescence in two immune phenotypes based on the expression of CD8+ T cells. (D) Correlation between the CD2 positive rate and CD8 positive rate detected using immunofluorescence. (E) Single cell level analysis evaluating the expression of CD2. ***$p < 0.001$.

sponse to type I interferon. The recruitment of CD8+ T cells to tumors is modulated by a variety of chemokines. Multiple chemokines are associated with the infiltration levels of CD8+ T cells in melanoma, such as the CCR5 ligands, CCL4 and CCL5, as well as the CXCR3 ligands, CXCL9 and CXCL10, which are interferon-responsive genes that have been shown to be activated in DC following the activation of type I interferon [60]. The stimulation of the Janus kinase-signal transducer and activator of transcription (JAK-STAT) pathway is necessary for the mediation of cellular responses to interferons. STAT proteins are known to be the primary signaling proteins for inflammatory cytokines, and they perform a critical role in the function and differentiation of immune cells [61]. Our study

demonstrated that the low-risk group was passively associated with several key chemokines and strongly enriched in the modulation of the immunity pathways, including JAK-STAT pathway and antigen processing and presentation, by using KEGG analysis. Moreover, the present study also indicated that higher CYT and GEP, both of which are strong anti-tumor immune effector signature and inflammation indicators, were observed in the low-risk group. Taken together, these findings illustrated that the low-risk group would shape the T cell–inflamed TME in HGSOC.

Numerous studies have shown that the presence of CD8+ T cells is correlated with the up-modulation of immunological inhibitory pathways, which are responsible for immune suppression. In the T-cell-inflamed TME, there are four primary immune evasion mechanisms: (i) PD-L1 up-modulation and subsequent T cells suppression via PD-L1 interaction with PD-1; (ii) IDO up-modulation; (iii) recruitment of regulatory T cells (Tregs) via CCL22 (produced from effector T cells); (iv) selection of tumor cells that have decreased antigenic immunogenicity [57]. As opposed to the T-cell inflammation TME, the TME with non-T-cell-inflammation has neither any T cells nor upmodulated immune suppressive mechanisms [58]. As a result, it should come as no surprise that checkpoint blocking is ineffective in this group of patients [62]. Our findings also imply that the low-risk group had an elevated level of immune checkpoint inhibitors and CCL22 as opposed to the high-risk group. The patients with low-risk scores tend to respond to ICB immunotherapy.

Aneuploidy has been shown to be correlated with diminished immune infiltration in a variety of tumor forms, according to the research literature [63]. The expressions of specific genes associated with cytotoxic actions facilitated by NK cells and CD8+ T cells were greatly decreased in tumors with high aneuploidy. Furthermore, genes involved in pathways that are associated with the existence of a continuous immune response and a cytokine-rich microenvironment were shown to be downregulated in high aneuploidy tumors [36]. These reports are consistent with what we have observed in the low-risk group. In our research, we discovered a strong positive correlation between risk signature and aneuploidy. Collectively, our findings indicate a decrease in immune-mediated pro-inflammatory and cytotoxic activity in the microenvironment of high-risk score tumors. When compared to non-HRD tumors, the response of HRD tumors to anti-neoplastic drugs such as platinum chemotherapy [64–66] or poly(ADP-ribose) polymerase (PARP) inhibitors [67,68] has been shown to be varied. We found the high-risk group tends to have lower HRD scores and acquire resistance to platinum-based chemotherapy in HGSOC. Moreover, defects in the HR pathway have been correlated with the activation of the stimulator of interferon genes (STING) pathway, which has been demonstrated to enhance the responses of antigen-specific T cell and transcription of type I interferon (IFN) genes in dendritic cells [69] and tumor cells [70]. This finding further corroborated our conclusion that the low-risk group may define a T cell-inflamed TME and exhibit a better response to ICB therapy.

CD2 is a well-recognized transmembrane glycoprotein belonging to the immunoglobulin superfamily, who expressed on the surface of dendritic cells, thymocytes, NK cells, and T cells [71,72]. Despite the fact that CD2 has been recognized for many years to be involved in a costimulatory pathway of T cell activation, studies of other costimulatory pathways with greater impact on mice have received considerable attention from immunologists up to now. Multiple studies showed that elevated expression of CD2 was correlated with the improved OS and distant metastasis-free survival in BRCA samples [73]. Our data indicated that elevated expression of CD2 resulted in an obviously longer FPS and OS. According to a recent research report, the downmodulation of CD2 could decrease the responses of anti-tumor T cells in colorectal and endometrial cancers, and even offset the efficacy of PD-1 immunotherapy in these cancers [74]. These reports are consistent with what we have observed in HGSOC by immunofluorescence. According to our findings, the infiltration levels of numerous effector TIICs, for example, CD8+ T cells and M1 macrophages, were considerably higher in the high-CD2 group, indicating that the expression of CD2 has an influence on the TME in HGSOC patients.

In spite of the fact that we have developed a prognostic signature and that our research gives new directions for improving HGSOC management, there exist a few drawbacks to this research. Firstly, the size of our sample and cell lines might be insufficient. Our external validation cohort only consisted of OS, which cannot further validate our signature effectively. The findings need to be validated by more independent cohorts to prove the clinical utility of risk model. Moreover, despite our efforts to elucidate the correlation between 9 LMRGs and immune infiltration, additional functional experiments are required to investigate the possible mechanisms in HGSOC. Lastly, there is currently no relevant dataset on HGSOC immunotherapy to validate the efficacy of our model and to screen HGSOC patients who may benefit from immunotherapy. Prospective clinical trials are recommended in order to further verify the clinical efficiency of the risk model in the context of ICB decisions.

5. Conclusions

We validated our results using two independent cohorts, which strengthened the robustness of our conclusion in terms of prognostic value of our 9 LMRGs prognostic signature. Our study identified the risk model of leukocyte migration associated with inflammatory TME in HGSOC and the role of the hub gene CD2 in TME, which may provide some potential clinical implications for comprehensive treatment of HGSOC. Meanwhile, CD2 may become a new

biomarker for predicting immune efficacy, and relevant experiments are needed to further confirm the key mechanism of CD2 regulation of TME.

Abbreviations

HGSOC, High-grade serous ovarian cancer; TME, tumor immune microenvironment; LMDGs, leukocyte migration-related differentially expressed genes; ssGSEA, single-sample gene set enrichment analysis; TIICs, tumor-infiltrating immune cells; PFS, progression-free survival; OS, overall survival; OC, Ovarian cancer; EOC, epithelial ovarian cancer; GO, gene ontology; NES, normalized enrichment score; FDR, false discovery rate; MHC, Major Histocompatibility Complex; GEP, T cell-inflamed gene expression profile; CYT, cytolytic activity; TCR, T cell receptor; BCR, B cell receptor; HRD, homologous recombination deficiency; MATH, Mutant-allele tumor heterogeneity; TMB, Tumor mutation burden; IC50, half-maximal inhibitory concentration; TIDE, Tumor Immune Dysfunction and Exclusion; IPS, immunophenoscore; IF, Immunofluorescence; PARP, poly(ADP-ribose) polymerase; GEPIA, Gene Expression Profiling Interactive Analysis.

Availability of Data and Materials

The public dataset used in this study is freely available at https://xenabrowser.net/ and https://www.ncbi.nlm.nih.gov/.

Author Contributions

The authors declare their contribution as follows. JP, XC and LY conceived and drafted of the manuscript. YS and JL assisted with data curation. LL and YL analyzed the data. SQ and LT participated in the formal analysis of the study. QX contributed to the concept, revised the article and provided project administration and funding acquisition. All authors have read and agreed to the published version of the manuscript.

Ethics Approval and Consent to Participate

Not applicable.

Acknowledgment

The results here are in whole or part based upon data generated by the TCGA Research Network: https://www.cancer.gov/tcga and the GEO Research Network: https://www.ncbi.nlm.nih.gov/geo/.

Funding

The project was funded by the grants of Joint Funds for the National Clinical Key Specialty Construction Program (2021); Innovative Medicine Subject of Fujian Provincial Health Commission (2020CX0101); Natural Science Foundation of Fujian Province (2020J011126); Fujian Provincial Clinical Research Center for Cancer Radiotherapy and Immunotherapy (2020Y2012).

Conflict of Interest

The authors declare no conflict of interest.

Supplementary Material

Supplementary material associated with this article can be found, in the online version, at https://doi.org/10.31083/j.fbl2806130.

References

[1] Lheureux S, Braunstein M, Oza AM. Epithelial ovarian cancer: Evolution of management in the era of precision medicine. CA: A Cancer Journal for Clinicians. 2019; 69: 280–304.

[2] Kim JY, Cho CH, Song HS. Targeted therapy of ovarian cancer including immune check point inhibitor. The Korean Journal of Internal Medicine. 2017; 32: 798–804.

[3] Peres LC, Cushing-Haugen KL, Köbel M, Harris HR, Berchuck A, Rossing MA, *et al*. Invasive Epithelial Ovarian Cancer Survival by Histotype and Disease Stage. Journal of the National Cancer Institute. 2019; 111: 60–68.

[4] Kim J, Park EY, Kim O, Schilder JM, Coffey DM, Cho CH, *et al*. Cell Origins of High-Grade Serous Ovarian Cancer. Cancers. 2018; 10: 433.

[5] Torre LA, Trabert B, DeSantis CE, Miller KD, Samimi G, Runowicz CD, *et al*. Ovarian cancer statistics, 2018. CA: A Cancer Journal for Clinicians. 2018; 68: 284–296.

[6] Ghisoni E, Imbimbo M, Zimmermann S, Valabrega G. Ovarian Cancer Immunotherapy: Turning up the Heat. International Journal of Molecular Sciences. 2019; 20: 2927.

[7] Ibrahim EM, Refae AA, Bayer AM, Sagr ER. Poly(ADP-ribose) polymerase inhibitors as maintenance treatment in patients with newly diagnosed advanced ovarian cancer: a meta-analysis. Future Oncology. 2020; 16: 585–596.

[8] Rossi L, Verrico M, Zaccarelli E, Papa A, Colonna M, Strudel M, *et al*. Bevacizumab in ovarian cancer: A critical review of phase III studies. Oncotarget. 2017; 8: 12389–12405.

[9] Kerliu L, Myruski S, Bhatti A, Soni P, Petrosius P, Pervanas HC, *et al*. Niraparib for the Treatment of Recurrent Epithelial Ovarian, Fallopian Tube, or Primary Peritoneal Cancer. The Annals of Pharmacotherapy. 2020; 54: 1010–1015.

[10] Zhang L, Conejo-Garcia JR, Katsaros D, Gimotty PA, Massobrio M, Regnani G, *et al*. Intratumoral T cells, recurrence, and survival in epithelial ovarian cancer. The New England Journal of Medicine. 2003; 348: 203–213.

[11] Lee JY, Kim JW, Lim MC, Kim S, Kim HS, Choi CH, *et al*. A phase II study of neoadjuvant chemotherapy plus durvalumab and tremelimumab in advanced-stage ovarian cancer: a Korean Gynecologic Oncology Group Study (KGOG 3046), TRU-D. Journal of Gynecologic Oncology. 2019; 30: e112.

[12] Nicolas-Boluda A, Donnadieu E. Obstacles to T cell migration in the tumor microenvironment. Comparative Immunology, Microbiology and Infectious Diseases. 2019; 63: 22–30.

[13] Entschladen F, Lang K, Drell TL, Joseph J, Zaenker KS. Neurotransmitters are regulators for the migration of tumor cells and leukocytes. Cancer Immunology, Immunotherapy. 2002; 51: 467–482.

[14] Cao JY, Guo Q, Guan GF, Zhu C, Zou CY, Zhang LY, *et al*. Elevated lymphocyte specific protein 1 expression is involved in the regulation of leukocyte migration and immunosuppressive microenvironment in glioblastoma. Aging. 2020; 12: 1656–1684.

[15] Leek JT, Johnson WE, Parker HS, Jaffe AE, Storey JD. The sva package for removing batch effects and other unwanted variation

in high-throughput experiments. Bioinformatics. 2012; 28: 882–883.
[16] Finotello F, Mayer C, Plattner C, Laschober G, Rieder D, Hackl H, *et al*. Molecular and pharmacological modulators of the tumor immune contexture revealed by deconvolution of RNA-seq data. Genome Medicine. 2019; 11: 34.
[17] Hänzelmann S, Castelo R, Guinney J. GSVA: gene set variation analysis for microarray and RNA-seq data. BMC Bioinformatics. 2013; 14: 7.
[18] Wilkerson MD, Hayes DN. ConsensusClusterPlus: a class discovery tool with confidence assessments and item tracking. Bioinformatics. 2010; 26: 1572–1573.
[19] Chakraborty H, Hossain A. R package to estimate intracluster correlation coefficient with confidence interval for binary data. Computer Methods and Programs in Biomedicine. 2018; 155: 85–92.
[20] Ritchie ME, Phipson B, Wu D, Hu Y, Law CW, Shi W, *et al*. limma powers differential expression analyses for RNA-sequencing and microarray studies. Nucleic Acids Research. 2015; 43: e47.
[21] Chen H, Boutros PC. VennDiagram: a package for the generation of highly-customizable Venn and Euler diagrams in R. BMC Bioinformatics. 2011; 12: 35.
[22] Engebretsen S, Bohlin J. Statistical predictions with glmnet. Clinical Epigenetics. 2019; 11: 123.
[23] Charoentong P, Finotello F, Angelova M, Mayer C, Efremova M, Rieder D, *et al*. Pan-cancer Immunogenomic Analyses Reveal Genotype-Immunophenotype Relationships and Predictors of Response to Checkpoint Blockade. Cell Reports. 2017; 18: 248–262.
[24] Chen DS, Mellman I. Oncology meets immunology: the cancer-immunity cycle. Immunity. 2013; 39: 1–10.
[25] Xu L, Deng C, Pang B, Zhang X, Liu W, Liao G, *et al*. TIP: A Web Server for Resolving Tumor Immunophenotype Profiling. Cancer Research. 2018; 78: 6575–6580.
[26] Ru B, Wong CN, Tong Y, Zhong JY, Zhong SSW, Wu WC, *et al*. TISIDB: an integrated repository portal for tumor-immune system interactions. Bioinformatics. 2019; 35: 4200–4202.
[27] Li T, Fu J, Zeng Z, Cohen D, Li J, Chen Q, *et al*. TIMER2.0 for analysis of tumor-infiltrating immune cells. Nucleic Acids Research. 2020; 48: W509–W514.
[28] Becht E, Giraldo NA, Lacroix L, Buttard B, Elarouci N, Petitprez F, *et al*. Estimating the population abundance of tissue-infiltrating immune and stromal cell populations using gene expression. Genome Biology. 2016; 17: 218.
[29] Li B, Severson E, Pignon JC, Zhao H, Li T, Novak J, *et al*. Comprehensive analyses of tumor immunity: implications for cancer immunotherapy. Genome Biology. 2016; 17: 174.
[30] Newman AM, Liu CL, Green MR, Gentles AJ, Feng W, Xu Y, *et al*. Robust enumeration of cell subsets from tissue expression profiles. Nature Methods. 2015; 12: 453–457.
[31] Singhania A, Graham CM, Gabryšová L, Moreira-Teixeira L, Stavropoulos E, Pitt JM, *et al*. Transcriptional profiling unveils type I and II interferon networks in blood and tissues across diseases. Nature Communications. 2019; 10: 2887.
[32] Auslander N, Zhang G, Lee JS, Frederick DT, Miao B, Moll T, *et al*. Robust prediction of response to immune checkpoint blockade therapy in metastatic melanoma. Nature Medicine. 2018; 24: 1545–1549.
[33] Rooney MS, Shukla SA, Wu CJ, Getz G, Hacohen N. Molecular and genetic properties of tumors associated with local immune cytolytic activity. Cell. 2015; 160: 48–61.
[34] Ott PA, Bang YJ, Piha-Paul SA, Razak ARA, Bennouna J, Soria JC, *et al*. T-Cell-Inflamed Gene-Expression Profile, Programmed Death Ligand 1 Expression, and Tumor Mutational Burden Predict Efficacy in Patients Treated With Pembrolizumab Across 20 Cancers: KEYNOTE-028. Journal of Clinical Oncology: Official Journal of the American Society of Clinical Oncology. 2019; 37: 318–327.
[35] Thorsson V, Gibbs DL, Brown SD, Wolf D, Bortone DS, Ou Yang TH, *et al*. The Immune Landscape of Cancer. Immunity. 2018; 48: 812–830.e14.
[36] Taylor AM, Shih J, Ha G, Gao GF, Zhang X, Berger AC, *et al*. Genomic and Functional Approaches to Understanding Cancer Aneuploidy. Cancer Cell. 2018; 33: 676–689.e3.
[37] Mroz EA, Rocco JW. MATH, a novel measure of intratumor genetic heterogeneity, is high in poor-outcome classes of head and neck squamous cell carcinoma. Oral Oncology. 2013; 49: 211–215.
[38] Mayakonda A, Lin DC, Assenov Y, Plass C, Koeffler HP. Maftools: efficient and comprehensive analysis of somatic variants in cancer. Genome Research. 2018; 28: 1747–1756.
[39] Yang W, Soares J, Greninger P, Edelman EJ, Lightfoot H, Forbes S, *et al*. Genomics of Drug Sensitivity in Cancer (GDSC): a resource for therapeutic biomarker discovery in cancer cells. Nucleic Acids Research. 2013; 41: D955–61.
[40] Jiang P, Gu S, Pan D, Fu J, Sahu A, Hu X, *et al*. Signatures of T cell dysfunction and exclusion predict cancer immunotherapy response. Nature Medicine. 2018; 24: 1550–1558.
[41] Santerre M, Chatila W, Wang Y, Mukerjee R, Sawaya BE. HIV-1 Nef promotes cell proliferation and microRNA dysregulation in lung cells. Cell Cycle. 2019; 18: 130–142.
[42] Shih AJ, Menzin A, Whyte J, Lovecchio J, Liew A, Khalili H, *et al*. Identification of grade and origin specific cell populations in serous epithelial ovarian cancer by single cell RNA-seq. PLoS ONE. 2018; 13: e0206785.
[43] Sun D, Wang J, Han Y, Dong X, Ge J, Zheng R, *et al*. TISCH: a comprehensive web resource enabling interactive single-cell transcriptome visualization of tumor microenvironment. Nucleic Acids Research. 2021; 49: D1420–D1430.
[44] Tsuiji H, Inoue I, Takeuchi M, Furuya A, Yamakage Y, Watanabe S, *et al*. TDP-43 accelerates age-dependent degeneration of interneurons. Scientific Reports. 2017; 7: 14972.
[45] McHugh ML. The chi-square test of independence. Biochemia Medica. 2013; 23: 143–149.
[46] Fujita M, Yamaguchi R, Hasegawa T, Shimada S, Arihiro K, Hayashi S, *et al*. Classification of primary liver cancer with immunosuppression mechanisms and correlation with genomic alterations. EBioMedicine. 2020; 53: 102659.
[47] Lu X, Jiang L, Zhang L, Zhu Y, Hu W, Wang J, *et al*. Immune Signature-Based Subtypes of Cervical Squamous Cell Carcinoma Tightly Associated with Human Papillomavirus Type 16 Expression, Molecular Features, and Clinical Outcome. Neoplasia. 2019; 21: 591–601.
[48] Baloch T, López-Ozuna VM, Wang Q, Matanis E, Kessous R, Kogan L, *et al*. Sequential therapeutic targeting of ovarian Cancer harboring dysfunctional BRCA1. BMC Cancer. 2019; 19: 44.
[49] Yu G, Li F, Qin Y, Bo X, Wu Y, Wang S. GOSemSim: an R package for measuring semantic similarity among GO terms and gene products. Bioinformatics. 2010; 26: 976–978.
[50] Tang Z, Li C, Kang B, Gao G, Li C, Zhang Z. GEPIA: a web server for cancer and normal gene expression profiling and interactive analyses. Nucleic Acids Research. 2017; 45: W98–W102.
[51] Biro M, Munoz MA, Weninger W. Targeting Rho-GTPases in immune cell migration and inflammation. British Journal of Pharmacology. 2014; 171: 5491–5506.
[52] Vicente-Manzanares M, Sancho D, Yáñez-Mó M, Sánchez-Madrid F. The leukocyte cytoskeleton in cell migration and immune interactions. International Review of Cytology. 2002; 216: 233–289.
[53] Di Vito C, Mikulak J, Zaghi E, Pesce S, Marcenaro E, Mavilio

D. NK cells to cure cancer. Seminars in Immunology. 2019; 41: 101272.
[54] Slaney CY, Kershaw MH, Darcy PK. Trafficking of T cells into tumors. Cancer Research. 2014; 74: 7168–7174.
[55] Susek KH, Karvouni M, Alici E, Lundqvist A. The Role of CXC Chemokine Receptors 1-4 on Immune Cells in the Tumor Microenvironment. Frontiers in Immunology. 2018; 9: 2159.
[56] Zhang Y, Xu L, Peng M. CXCR3 is a prognostic marker and a potential target for patients with solid tumors: a meta-analysis. OncoTargets and Therapy. 2018; 11: 1045–1054.
[57] Spranger S. Mechanisms of tumor escape in the context of the T-cell-inflamed and the non-T-cell-inflamed tumor microenvironment. International Immunology. 2016; 28: 383–391.
[58] Spranger S, Spaapen RM, Zha Y, Williams J, Meng Y, Ha TT, *et al*. Up-regulation of PD-L1, IDO, and T(regs) in the melanoma tumor microenvironment is driven by CD8(+) T cells. Science Translational Medicine. 2013; 5: 200ra116.
[59] Gajewski TF. The Next Hurdle in Cancer Immunotherapy: Overcoming the Non-T-Cell-Inflamed Tumor Microenvironment. Seminars in Oncology. 2015; 42: 663–671.
[60] Harlin H, Meng Y, Peterson AC, Zha Y, Tretiakova M, Slingluff C, *et al*. Chemokine expression in melanoma metastases associated with CD8+ T-cell recruitment. Cancer Research. 2009; 69: 3077–3085.
[61] Morris R, Kershaw NJ, Babon JJ. The molecular details of cytokine signaling via the JAK/STAT pathway. Protein Science: a Publication of the Protein Society. 2018; 27: 1984–2009.
[62] Tumeh PC, Harview CL, Yearley JH, Shintaku IP, Taylor EJM, Robert L, *et al*. PD-1 blockade induces responses by inhibiting adaptive immune resistance. Nature. 2014; 515: 568–571.
[63] Davoli T, Uno H, Wooten EC, Elledge SJ. Tumor aneuploidy correlates with markers of immune evasion and with reduced response to immunotherapy. Science. 2017; 355: eaaf8399.
[64] Loibl S, Weber KE, Timms KM, Elkin EP, Hahnen E, Fasching PA, *et al*. Survival analysis of carboplatin added to an anthracycline/taxane-based neoadjuvant chemotherapy and HRD score as predictor of response-final results from GeparSixto. Annals of Oncology: Official Journal of the European Society for Medical Oncology. 2018; 29: 2341–2347.
[65] Safra T, Rogowski O, Muggia FM. The effect of germ-line BRCA mutations on response to chemotherapy and outcome of recurrent ovarian cancer. International Journal of Gynecological Cancer. 2014; 24: 488–495.
[66] Mota JM, Barnett E, Nauseef JT, Nguyen B, Stopsack KH, Wibmer A, *et al*. Platinum-Based Chemotherapy in Metastatic Prostate Cancer With DNA Repair Gene Alterations. JCO Precision Oncology. 2020; 4: 355–366.
[67] Moore K, Colombo N, Scambia G, Kim BG, Oaknin A, Friedlander M, *et al*. Maintenance Olaparib in Patients with Newly Diagnosed Advanced Ovarian Cancer. The New England Journal of Medicine. 2018; 379: 2495–2505.
[68] Robson M, Im SA, Senkus E, Xu B, Domchek SM, Masuda N, *et al*. Olaparib for Metastatic Breast Cancer in Patients with a Germline BRCA Mutation. The New England Journal of Medicine. 2017; 377: 523–533.
[69] Corrales L, Gajewski TF. Molecular Pathways: Targeting the Stimulator of Interferon Genes (STING) in the Immunotherapy of Cancer. Clinical Cancer Research: an Official Journal of the American Association for Cancer Research. 2015; 21: 4774–4779.
[70] Pantelidou C, Sonzogni O, De Oliveria Taveira M, Mehta AK, Kothari A, Wang D, *et al*. PARP Inhibitor Efficacy Depends on $CD8^+$ T-cell Recruitment via Intratumoral STING Pathway Activation in BRCA-Deficient Models of Triple-Negative Breast Cancer. Cancer Discovery. 2019; 9: 722–737.
[71] Krensky AM, Sanchez-Madrid F, Robbins E, Nagy JA, Springer TA, Burakoff SJ. The functional significance, distribution, and structure of LFA-1, LFA-2, and LFA-3: cell surface antigens associated with CTL-target interactions. Journal of Immunology. 1983; 131: 611–616.
[72] Matsui T, Connolly JE, Michnevitz M, Chaussabel D, Yu CI, Glaser C, *et al*. CD2 distinguishes two subsets of human plasmacytoid dendritic cells with distinct phenotype and functions. Journal of Immunology. 2009; 182: 6815–6823.
[73] Chen Y, Meng Z, Zhang L, Liu F. CD2 Is a Novel Immune-Related Prognostic Biomarker of Invasive Breast Carcinoma That Modulates the Tumor Microenvironment. Frontiers in Immunology. 2021; 12: 664845.
[74] Demetriou P, Abu-Shah E, Valvo S, McCuaig S, Mayya V, Kvalvaag A, *et al*. A dynamic CD2-rich compartment at the outer edge of the immunological synapse boosts and integrates signals. Nature Immunology. 2020; 21: 1232–1243.